Available online at www.sciencedirect.com
ScienceDirect
Applied Catalysis B: Environmental 80 (2008) 214–225
APPLIED CATALYSIS B: ENVIRONMENTAL
www.elsevier.com/locate/apcatb

Pt–Ba–Al_2O_3 for NO_x storage and reduction: Characterization of the dispersed species

Irene Malpartida [a], Maria Angeles Larrubia Vargas [a], Luis J. Alemany [a], Elisabetta Finocchio [b], Guido Busca [b,*]

[a] *Departamento de Ingeniería Química, Universidad de Málaga, 29071 Málaga, Spain*
[b] *DIChePI, Università di Genova, P.le J.F. Kennedy 1, I-16129 Genova, Italy*

Received 13 September 2007; received in revised form 20 November 2007; accepted 24 November 2007
Available online 1 February 2008

Abstract

Pt–Ba–Al_2O_3 active and selective for NO_x storage and selective reduction to N_2 has been prepared and tested. Characterization of the parent Al_2O_3, Pt–Al_2O_3 and Ba–Al_2O_3 materials, as well as of Pt–Ba–Al_2O_3 catalyst in the oxidized, reduced and sulphated state has been performed by FT-IR spectroscopy of low-temperature adsorbed carbon monoxide and of adsorbed acetonitrile. XRD, TEM and XPS analyses have also been performed. Evidence for the predominance of Ba species, which are highly dispersed on the alumina support surface, and may be carbonated or sulphated, has been provided. Competitive interaction of Pt and Ba species with the surface sites of alumina has also been found.

Keywords: NO_x storage and reduction; Pt–Ba–Al_2O_3 catalysts; IR spectroscopy; CO adsorption; TEM Pt–Ba–Al_2O_3; XPS Pt–Ba–Al_2O_3; Sulfation NSR catalysts

1. Introduction

NO_x storage–reduction (NSR) is a recent technology, first developed by Toyota in the early 1980s [1,2], to reduce the NO_x content in waste gases of lean-burn gasoline and diesel engines. A following evolution of this technology is the newer diesel particulate-NO_x reduction (DPNR) process, also developed by Toyota [3,4]. It allows the simultaneous abatement of both particulate and NO_x due to the development of a new catalytic filter and a new diesel combustion technology.

The catalytic materials for both NSR [5] and DPNR consist in porous ceramic filters coated with a catalytic layer constituted by a high surface area support (typically γ-alumina), a noble metal (usually Pt) and an alkaline or alkali-earth metal oxide which presents a high NO_x-storage capacity, most frequently Ba oxide. These catalytic systems work under cyclic conditions, alternating long lean phases (during which NO_x are adsorbed on the catalyst in the form of nitrate/nitrites) with short phases in rich condition (during which the nitrate–nitrite species are reduced to molecular nitrogen). Several studies have been devoted to the investigation of the reaction mechanisms of the $DeNO_x$ steps (adsorption/reduction) over these systems, including infrared studies [6–12]. The results do not seem, however, to agree completely.

One of the limits of these studies is due to the still imperfect knowledge of the surface chemistry of the catalytic materials. Although γ-Al_2O_3 is one of the most largely used and studied materials as a whole, even its bulk structure, either a cubic defective spinel [13,14] or a structure based on ccp oxide lattice but different from and more stable than that of a spinel [15], is still under debate. Also the surface properties of alumina are still not fully understood, as recently underlined by Lambert and Che [16], and several investigations are still appearing in the open literature [14,17–20]. Much less is known, consequently, on the details of the surface chemistry and structure of BaO/γ-Al_2O_3 and Pt–BaO/γ-Al_2O_3. Several studies reveal that these materials, when fresh, present barium carbonate $BaCO_3$ as an evident bulk component. In the contact with the waste gas of lean-burn engine, however, where NO_x and SO_2 are present, barium nitrate $Ba(NO_3)_2$ and barium sulphate $BaSO_4$ may be detected.

The IR spectroscopy of low-temperature adsorption of CO is today a very popular technique for the characterization of solid surfaces [21,22]. This is because CO is a very good and gentle probe for surface hydroxy groups, cationic and metallic centers,

* Corresponding author. Tel.: +39 010 353 60 24; fax: +39 010 353 60 24.
E-mail address: Guido.Busca@unige.it (G. Busca).

0926-3373/$ – see front matter © 2007 Elsevier B.V. All rights reserved.
doi:10.1016/j.apcatb.2007.11.035

with small or no surface perturbation. Room temperature CO adsorption on Pt–BaO/γ-Al_2O_3 has been the object of few recent studies [6,8]. Both these studies report a complex chemistry of CO on the surface, with the formation of reactive adsorption carbonate-like species. This reactivity prevented the use of CO as a probe of the clean catalyst surface structure. We present here a low-temperature CO adsorption IR study, coupled with XRD, XPS and TEM investigations, in order to have a better description of the surface chemistry of the catalytic materials for NSR.

2. Experimental

2.1. Catalyst preparation

The support (hereinafter denoted as A) is γ-alumina (S_{BET} = 250 m^2/g, V_p = 1.045 cm^3/g) obtained by calcination of a pseudoboehmite precursor at 500 °C for 2 h. The incorporation of Ba and Pt onto the support was made by incipient wetness impregnation method using aqueous solutions of the barium acetate ($Ba(CH_3COO)_2$, Merck), and diamminedinitritoplatinum(II) ($Pt(NH_3)_2(NO_2)_2$, Aldrich). For Pt–Ba–Al_2O_3 catalysts (PtBaA) the impregnation has been performed in two separate consecutive steps: first, Pt was dispersed onto the carrier, dried overnight at 90 °C and calcined in air at 300 °C during 3 h to stabilize the first metal incorporated. Then, barium was incorporated by an impregnation of the activated Pt/Al_2O_3 (PtA). The sample was dried again and calcined in air at 500 °C during 2 h. The metal loading, expressed as formal surface atomic density (atoms per nanometre square, at/nm^2), is 0.4 at-Pt/nm^2 and 5 at-Ba/nm^2 for both mono- and bi-metallic samples.

2.2. X-ray diffraction

X-ray diffraction patterns of the samples were recorded using a Siemens D-501 diffractometer using Cu Kα radiation (40 kV, 22.5 mA).

2.3. XPS characterization

Photoelectron spectra were recorded over fresh samples using a Physical Electronic 5700 spectrometer equipped with a hemispherical electron analyzer operating with a Mg Kα X-ray exciting source (1253.6 eV, 15 kV, 300 W). The binding energies (BE) were referenced to the C 1s peak, used as an internal patron for calibration and fixed at 284.8 eV considering a deviation ±0.2 eV. Consequence of the asymmetry presented by the signals registered for O 1s, Ba $3d_{5/2}$, C 1s, Pt $4d_{5/2}$ regions, the bands are the result of the contribution of more than one species and the relative population have been determined by deconvolution. A strategy was developed for the mathematical deconvolution; in all cases the signal was adjusted to a mathematical response consistent of a Gaussian–Lorenztian distribution (80–20%, respectively) with a minimal χ^2 deviation. The references values were taken from the NIST X-ray photoelectron spectroscopy database [23].

2.4. Transmission electron microscopy

Transmission electron micrographs (TEM) were recorded using a Philips CM 200 instrument (200 kV).

2.5. Catalytic experiments

NO_x abatement has been investigated over the PtBaA catalyst under transient conditions using a flow system with a quartz tube reactor (7 mm i.d.) directly coupled to a MS (Mass Spectrometer, Balzers QMS 200). Catalyst loaded into reactor was 0.120 g (<200 mesh) and it is previously activated at 500 °C in 20% O_2 in He atmosphere (200 cm^3/min). The temperature was set at 350 °C in a stream of He containing 3% O_2. After stabilization of MS signals, a rectangular pulse of 1000 ppm NO (containing Ar as internal reference, i.r.) was admitted to the reactor until saturation of catalyst; then, the NO_x concentration was decrease back to zero. The NO_x species adsorbed during the pulse were removed by feeding a stream of 2000 ppm H_2 (with Ar as i.r.) in He. Simultaneously, the reactor gas-off was monitored as temporal evolution following the *m*/*e* ratios: 2 (H_2), 15 (NH_3), 18 (H_2O), 28 (N_2), 30 (NO), 32 (O_2), 40 (Ar), 44 (N_2O or CO_2) and 46 (NO_2). The quantitative results are shown as NO_x conversion that is calculated as the integral difference between the inlet and outlet NO concentrations on the adsorption step and in terms of N_2-selectivity during the regeneration step.

2.6. FT-IR characterization

In situ transmission FT-IR spectra were collected on a Nicolet Nexus instrument. Self-supporting pressed disks of pure catalysts powders were activated in the IR cell by outgassing at 500 °C during 1 h before the adsorption experiments. Besides, the platinum containing samples were activated in H_2 atmosphere (500 Torr) at 500 °C during 30 min with a subsequent evacuation by outgassing at 500 °C during 30 min in order to compare the reduced and non-reduced spectra. Sulphated PtBaA (PtBaAS) has been prepared by contacting the catalyst with a very small pressure of SO_2 (<0.1 Torr) at 773 K in the IR cell. A conventional gas manipulation/outgassing ramp was connected to a IR cell which allowed cooling by liquid nitrogen in an external jacket. CO adsorption has been performed at 140 K (real sample temperature measured by a thermocouple) by the introduction of a known dose of CO gas. IR spectra were collected evacuating and warming between 140 K and room temperature (r.t.) and some cases up to 100 °C.

3. Results

3.1. XRD analyses

Fig. 1 left shows the XRD-spectra of the support, monometallic and bimetallic catalysts. The XRD pattern of the support only shows weak diffraction peaks at 37° and 45° associated to γ-Al_2O_3 (JCPDS 04-0880). The peak at 44° (2θ) is

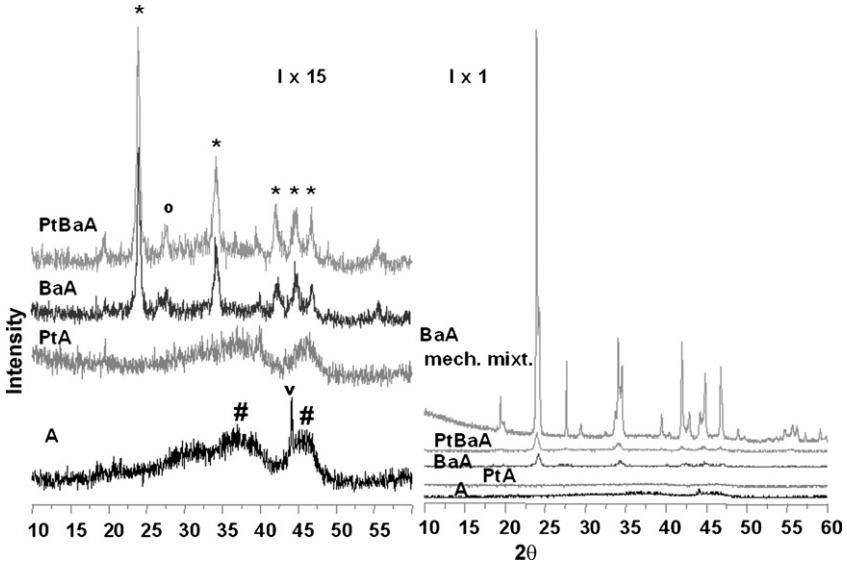

Fig. 1. XRD patterns of fresh catalysts. In the left side the pattern of a mechanical mixture of $BaCO_3$–γ-Al_2O_3 having the same Ba:Al_2O_3 composition of BaA is added. The intensity scale in the right side is 15 times that of the left part.

due to the sampling cup. No diffraction peaks due to formation of platinum species were observed for all calcined samples. For barium containing catalysts, the signal at 24.3° (2θ) and several other peaks are associated with orthorhombic $BaCO_3$ (witherite, JCPDS 05-0378), isostructural with aragonite; in addition traces of monoclinic $BaCO_3$ are also detected at 27° (JCPDS 78-2057). Interestingly, the pattern of $BaCO_3$ is slightly stronger in the case of Pt-containing catalyst PtBaA than on the ''monometallic'' BaA powder. The right part of Fig. 1 shows the same XRD patterns together with that of a mechanical mixture of $BaCO_3$ and γ-Al_2O_3 having the same virtual composition of BaA. The intensity scale is different, being 15 times expanded. The intensity of the pattern due to $BaCO_3$ is 20 times stronger in the mechanical mixture than in the catalysts. This means that only near 5% of Ba in the catalysts is in the form of bulk $BaCO_3$ particles, while 95% is not detected by XRD, being likely dispersed on the surface. These data fully agree with those reported by Lietti et al. [24]. According to this evaluation, the contribution to the overall catalyst surface of bulk $BaCO_3$ particles is almost negligible, while that of dispersed Ba^{2+} ions may be relevant. Taking into account the virtual surface density of Ba^{2+}, 5 at/nm^2, we can calculate that the density of dispersed Ba^{2+} ions may be near 4.75 at/nm^2 of the catalyst surface, which corresponds to near 21 Å^2 per Ba ion. Taking into account that the ionic radius of both Ba^{2+} and O^{2-} ions are in the range 1.36–1.42 Å [25] it is easy to calculate that the coverage of the alumina surface by dispersed Ba oxide or carbonate species approaches to be complete. On the other hand, the crystal size of the bulk $BaCO_3$ phase in the BaA and PtBaA catalysts is measured, using the Sherrer formula, to be near 100 nm, taking into account the density of $BaCO_3$ (4308 g/cm^3), we can calculate that the surface area of the bulk $BaCO_3$ phase is negligible in the fresh catalyst, contributing to less than 0.5% of the total catalyst area.

These data show that at least two Ba species exist on the fresh catalyst. Most of Ba is XRD undetectable, likely being dispersed on the surface in the form of something can be called ''a monolayer'', while only a very small fraction forms a XRD detected bulk $BaCO_3$ phases. This conclusion roughly agrees with the conclusions of Lietti et al. [24], Piacentini et al. [26] and Scholz et al. [27], both finding different Ba species on the surface of similar catalysts.

3.2. XPS spectra

The values of binding energies of Al 2p, Ba $3d_{5/2}$ and Pt $4d_{5/2}$ core electrons for the fresh catalytic materials are listed in Table 1. The binding energy of Al 2p at ca. 73.8–74 eV is related to the γ-Al_2O_3 support, according to the literature [28]. For the catalysts with Ba, the binding energy of Ba $3d_{5/2}$ at 780.5 eV reveals that Ba is present mainly as carbonate. It seems likely that this technique does not distinguish the contribution of surface Ba carbonate, that according the previous discussion is largely predominant, with bulk $BaCO_3$ particles, whose amount is much lower. A second Ba XPS component is detected at smaller binding energies (779.8–779.9 eV), which is associated with traces of an oxide phase

Table 1
XPS peaks positions

Catalyst	Binding energies (eV)		
	Al 2p	Ba $3d_{5/2}$	Pt $4d_{5/2}$
A	74.0		
PtA	74.0		314.9 (50) 317.1 (49) 318.5 (<1)
BaA	73.8	779.8 (2) 780.5 (98)	
PtBaA	74.0	779.9 (9) 780.5 (91)	314.5 (67) 317.2 (32) 318.4 (1)

(BaO-like) [29]. For platinum, only the Pt $4d_{5/2}$ was recorded, because the most intense Pt 4f peak was overlapped by a very strong Al 2p peak; this is usual with alumina-supported catalysts [29–31]. The binding energy of Pt $4d_{5/2}$ for the monometallic sample, PtA, and the peak intensity indicate that the 50% of Pt is present as Pt^0 (314.9 eV) [31,32] upon XPS measurement. In the case of the bimetallic catalyst, PtBaA, the binding energy of Pt^0 is shifted slightly (314.5 eV) and the peak is stronger. A second Pt component is observed at higher binding energies (317.1 ± 0.1 eV) corresponding to an oxidized species of Pt (Pt^{2+}) [30]. A weak tail in the signal revealed a higher binding energy component (318.4 ± 0.1 eV), that can be associated to the presence of traces of Pt in a even higher oxidation state (Pt^{4+}) [30], upon XPS measurement. Modifications of the binding energies of platinum and the different amounts of the different oxidation states would be indicative of the existence of interaction effect when barium is present in the formulation. A similar interaction of platinum with others metals (Pt–Ce and Pt–Ti) is registered in bibliography [31,32]. These data are consistent with the previous ones of Anderson et al. [10] and Casapu et al. [33].

3.3. Transmission electron microscopy

TEM images of the monometallic PtA catalyst are shown in Fig. 2. The alumina support appears as very elongated particles, some tens of nanometers long, few nanometers thin. The morphology observed for this alumina is typical of materials obtained by (pseudo)bohemite decomposition as well as of the parent oxy-hydroxide [34,35], revealing the lamellar or nanofibrous structure of γ-AlOOH that are at least partly preserved after topotactic transformation into γ-Al_2O_3. The few darker particles having a more defined globular structure are due to noble metal particles, which were well distributed in the alumina powder. The size of these Pt particles was determined to be around 10 nm. However, smaller dark dots suggest that smaller Pt particles, of few nm sizes, may also exist. The TEM micrographs of PtBaA are similar to those of PtA.

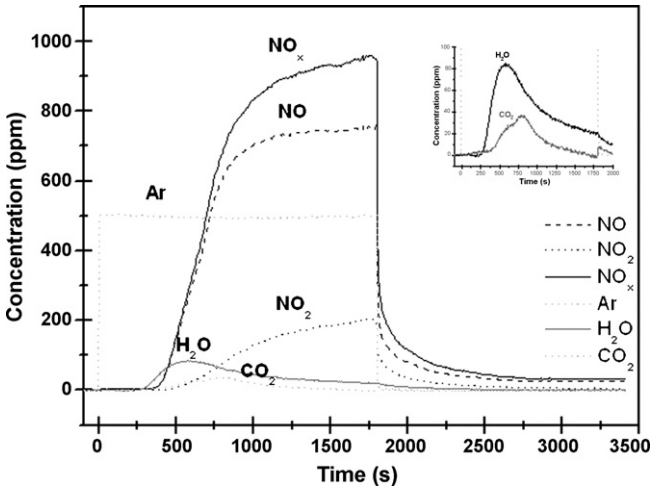

Fig. 3. Gas phase compositions measured during and after the NO_x adsorption pulse (0–1800 s) over PtBaA.

3.4. Catalytic activity

In Fig. 3 the data relative to the NO_x adsorption experiments on the PtBaA catalyst are reported. The out-flow NO_x gas concentration is zero since the beginning of the pulse until 437 s (corresponding to a complete adsorption by the BaO component of the catalyst), increasing later up to more than 950 ppm at the end of the pulse (1800 s, Fig. 3), mostly due to NO. After 250 s an evolution of water is registered and CO_2 is observed in the interval of 400–1250 s. The formation of H_2O and CO_2 during the storage stage indicates that the different Ba phases active in the storage of NO_x are first as BaO, then as

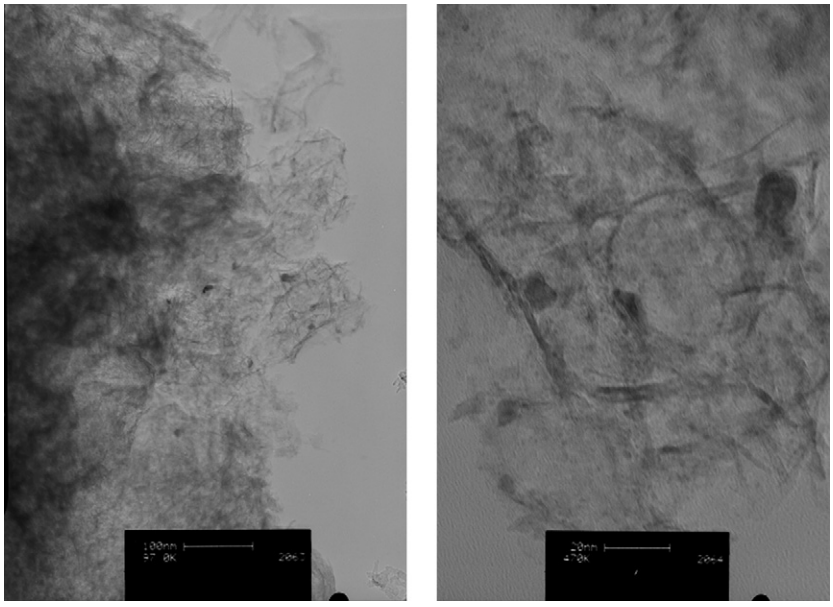

Fig. 2. TEM images of PtA: magnifications 97,000 left, 470,000 right.

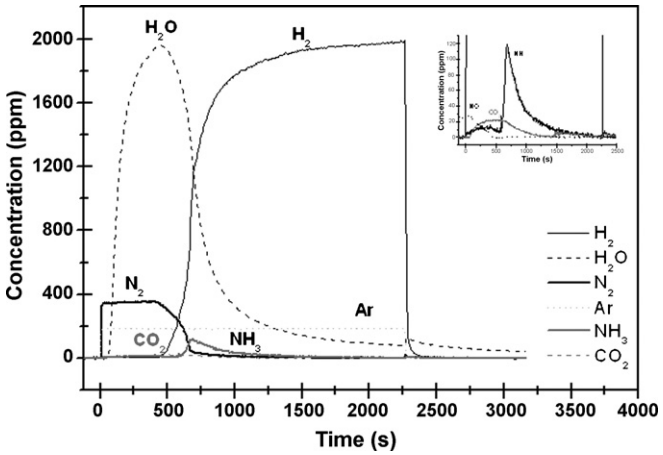

Fig. 4. Gas phase compositions measured during and after the H_2 reduction step (pulse 0–2250 s) over PtBaA.

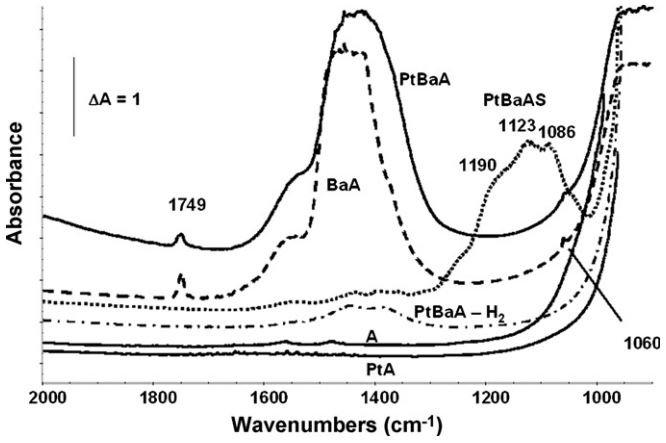

Fig. 5. FT-IR spectra of the samples, all after outgassing at 773 K.

$Ba(OH)_2$ (or a highly hydroxylated part of the surface), finally a carbonated part of the surface, mostly surface $BaCO_3$. Also we can see in the figure of the reduction stage that there is a delay in the water evolution with respect to the N_2 evolution. This is associated with the hydroxylation of barium oxide. After the end of the rectangular pulse the concentration of NO_x drops rapidly down to low but not zero values. A tail due to NO desorption is still observed after 3400 s.

During the regeneration step (Fig. 4), just after the beginning of the H_2 pulse, water, N_2 and very small amounts of CO_2 are released, hydrogen being fully consumed. After 500 s hydrogen consumption and water and nitrogen release decrease. A small peak of ammonia release (120 ppm maximum) is observed. Release of NO is very small, only at the beginning of the hydrogen pulse. This shows that this catalyst is active and highly selective in the adsorption and reduction of NO_x to N_2. The selectivity measured upon the reduction step is 89%.

The amounts of Ba participating in the process can be calculated from the amounts of NO_x species adsorbed during the storage period, supposing the formation of either $Ba(NO_2)_2$ or $Ba(NO_3)_2$ (i.e. a NO_{xads}/Ba_{active} ratio of 2). The amount of NO_x species stored until the breakthrough time (complete NO_x storage, 370 s) is 4.45×10^{-4} mol/g and until catalyst saturation is 7.84×10^{-4} mol/g. This means that for a complete NO_x abatement around 11% of barium is active and the fraction of barium involved until saturation is about 19%. This is in line with the suggestions of Castoldi et al. [36] that the maximum storage capacity is around 25% and presented by the systems which are characterized by the formation of the monolayer.

3.5. IR study: catalysts activation

In Fig. 5 the spectra of the samples after activation in vacuum have been reported. All spectra present the typical features of the pressed disks of alumina-based materials, with a moderately increasing baseline towards higher energies due to light scattering, and a sharp cut-off near 1000 cm^{-1} due to bulk Al–O absorptions. PtA absorbs less than A in the region 1100–1000 cm^{-1} due to the perturbation of surface Al–O–Al bonds. The spectra of the Ba-containing samples present an additional very strong band in the range 1500–1400 cm^{-1}, and very weak peaks at 2450, 1749 and 1060 cm^{-1}. The strong band at 1500–1400 cm^{-1} is associated to the asymmetric CO stretching ($\nu 3$) of carbonate ions, while the feature at 1060 cm^{-1} is due to the corresponding symmetric stretching ($\nu 1$). The former mode is IR and Raman active (E′ symmetry) but the latter is IR inactive and Raman active (A_1' symmetry) in the fully symmetrical trigonal-planar carbonate ions (D_{3h} point group). However, in the case of the aragonite-type bulk carbonates (space group $Pmnc = D_{2h}^{16}$, with $Z = 4$), like witherite (i.e. orthorhombic $BaCO_3$), the coupling of the vibrations of the four carbonate ions present in the primitive cell [37,38] gives rise to three nearly coincident IR active modes arising from $\nu 3$ ($B_{1u} + B_{2u} + B_{3u}$), found very strong at 1449 cm^{-1}, and two nearly coincident IR active modes arising from $\nu 1$ ($B_{1u} + B_{3u}$), found also well evident at 1059 cm^{-1} [39,40]. The weakness of the band at 1060 cm^{-1} in our case shows that bulk witherite particles are in fact only in small part responsible for the bands of carbonate ions, in agreement with the small amount of this phase detected by XRD. Most of the band at 1500–1400 cm^{-1} is due to carbonate ions still almost symmetrical but not belonging to bulk $BaCO_3$ particles. Additionally, we observe also pronounced components at both sides of the main degenerate $\nu 3$ band, due to the splitting of $\nu 3$ of less symmetric surface carbonates species, such as e.g. bidentate or bridging. The peaks at 1749 and 2450 cm^{-1} are due to combination modes of the trigonal carbonate ions ($\nu 1 + \nu 4$ and $\nu 1 + \nu 3$, respectively). These features are frequently observed in the spectra of Ba-containing oxides [41].

The bands of both bulk and surface carbonate species almost disappeared after reduction of PtBaA in hydrogen, showing that in these conditions carbonates may be reduced (e.g. to methane) and/or decomposed to give gas-phase CO_2, likely producing dispersed and possibly microcrystalline bulk Ba oxide species.

3.6. Surface hydroxyl groups and CO adsorption on γ-Al_2O_3

In Fig. 6 the IR spectra of the surface hydroxy groups of the samples are enlarged. The spectrum of alumina (A) is quite

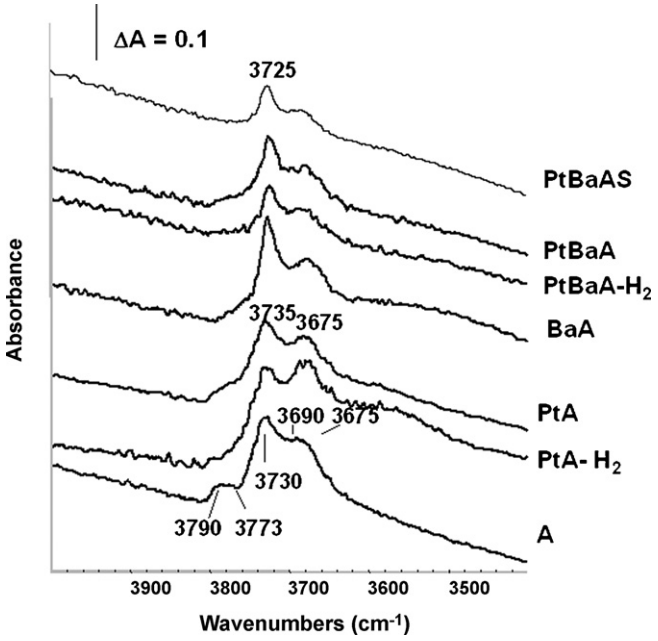

Fig. 6. FT-IR spectra of the samples, all after outgassing at 773 K, in the OH stretching region.

typical for γ-Al_2O_3 samples. The strongest band is observed at 3730 cm^{-1}, while weaker bands are poorly resolved at higher frequency, near 3790 and 3770 cm^{-1}, and a broader shoulder possibly constituted by two components near 3690 and 3675 cm^{-1} is evident at lower frequencies.

In Fig. 7 the spectra of carbon monoxide adsorbed on sample A (γ-Al_2O_3) are reported. At the highest coverages (in the insert in Fig. 7) the main maximum is at 2144 cm^{-1} and could be assigned to very weakly physisorbed CO. After outgassing upon warming Two main features are observed, both shifting upwards by increasing outgassing temperature. The most intense νCO band at high coverages, due to a more weakly held species, disappears faster and shifts from near 2154 cm^{-1} to near 2160 cm^{-1}. The other band, more resistant to outgassing,

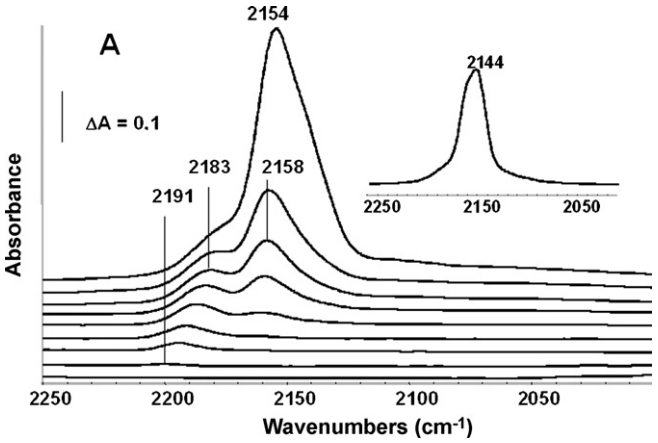

Fig. 7. FT-IR spectra of CO adsorbed on A at 140 K, after outgassing at increasing temperatures from 140 K to 230 K (from up to down). In the insert: in contact with CO gas at 140 K. The spectrum of the activated catalyst has been subtracted.

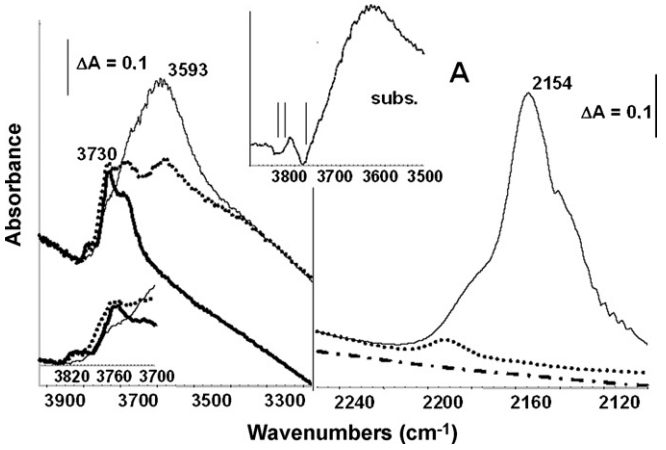

Fig. 8. FT-IR spectra of A (left, OH stretching region), and of CO adsorbed on A (right), after activation (heavy line), after short contact with CO at 140 K (light line) and after outgassing at 190 K (point line) and at 230 K (dashed line).

shifts from near 2180 to 2191 cm^{-1}. Looking at the OH stretching region (Fig. 8) it is evident that the νCO band at 2154–2160 cm^{-1} is associated to the H-bonding of CO with surface hydroxy groups. Upon this interaction, the two higher frequency νOH bands are almost totally disappeared, while the band at 3730 cm^{-1} is involved partially. The component at 3675 cm^{-1} seems almost not involved, being still evident as a shoulder. The shift of the OH stretching band is, consequently, in the range $\Delta\nu OH \sim 200–140\ cm^{-1}$, which allows to denote the alumina's OH as medium strength Brønsted acid sites. The band shifting from near 2180 to 2191 cm^{-1}, instead, does not correspond to any perturbation of the νOH bands. It is assigned to CO species interacting with Lewis acidic Al^{3+} cations. The shift with respect to νCO of gas or liquid CO is relatively weak, and this shows that after outgassing at 773 K the strongest Lewis sites of alumina are still not produced. The surface is still in a highly hydroxylated state. The persistency of an absorption in the region below 3650 cm^{-1} is associated to the formation of extremely small amounts of carbonate, bicarbonate and formate species, evident form the expansion of the subtraction spectra in the region 1700–1200 cm^{-1}, showing that very few reactive sites are present on this surface.

3.7. Surface hydroxy groups and CO adsorption on Pt–γ-Al_2O_3

The spectrum of the PtA catalyst in the νOH region (Fig. 6) shows the main band almost with the same intensity than on alumina but shifted upwards a little bit (3735 cm^{-1}), while the two components at higher frequency are definitely decreased in intensity. The component at the lowest frequency (3675 cm^{-1}) is a little increased in intensity. After reduction in hydrogen, the two higher frequency components are fully disappeared but the absorption at the lower frequency side is increased, with the appearance of a new component, broad, at 3550 cm^{-1}.

The spectra of CO adsorbed on PtA sample with and without prereduction are shown in Fig. 9. The addition of Pt to alumina causes the formation of a new νCO band which is observed in the range 2100–2000 cm^{-1} in both cases, typical for terminal

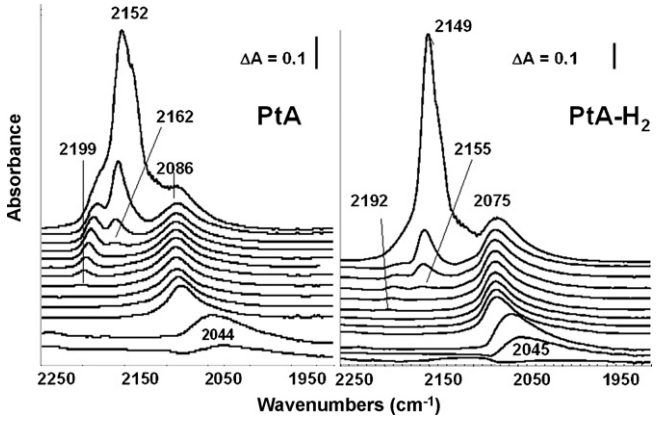

Fig. 9. FT-IR spectra of CO adsorbed on PtA, unreduced (left) and reduced (right) at 140 K in contact with CO gas, and after outgassing at increasing temperatures from 140 K to 273 K (from up to down). The very last spectrum is recorded after outgassing at 373 K. The spectrum of the activated catalyst has been subtracted.

Pt^0 carbonyls [42]. This band is near 2085 cm^{-1} in the unreduced sample, while is near 2075 cm^{-1} in the prereduced sample. By outgassing upon warming, this band is first quite stable while, when it begins to decrease in intensity; in both cases it shifts significantly downwards to near 2040 cm^{-1}, now very broad.

The positions of the peak observed both at the highest CO coverages (2085–2075 cm^{-1}) and at the lowest coverages (~2040 cm^{-1}) is in line with that observed for alumina supported Pt particles whose average size is of the order of few nanometers, which should be further smaller for the hydrogen reduced sample [42]. This confirms that, together with the few particles having a size of the order of 10 nm, several smaller particles envisaged with difficulty from TEM micrographs, are predominant.

The other two bands (i.e. ~2195 and ~2150 cm^{-1}) behave, on PtA, in a similar way than on A, but the highest frequency band is definitely more intense and shifted at higher frequency for unreduced PtA than for reduced PtA and for A.

In Fig. 10 the spectra of CO adsorbed on reduced and unreduced PtA are compared in the same scale. The much higher strength before reduction of the component near 2198 cm^{-1} is evident, while the higher intensity and the shift downwards of the band of Pt^0 carbonyls after reduction can also be observed. This comparison suggests that at least part of the band observed at 2198 cm^{-1} may be due to νCO of Pt^{4+}–CO species [22], which are reduced during treatment in hydrogen. The shift down upon reduction of νCO of Pt^0–CO species may be due to a better dispersion obtained after reduction [42] while the shift down upon outgassing is a usual phenomenon, attributed to the decrease of dipole–dipole coupling by decreasing the coverage.

Looking at the spectrum of the surface hydroxy groups (Figs. 11 and 12), the main band at ~2150 cm^{-1} is again associated to the shift of the OH stretching band at ~3735 cm^{-1} down to ~3620 cm^{-1} both without and with reduction. This shows that the OH stretching band observed at 3735 cm^{-1} for PtA is associated to hydroxy groups whose Brønsted acidity is lower than that of the hydroxy groups found on alumina. In fact the shift ($\Delta\nu$OH ~ 115 cm^{-1}) is lower than that observed on alumina.

3.8. Surface hydroxy groups and CO adsorption on Ba–γ-Al_2O_3

The BaA sample (Fig. 6) shows a spectrum in the OH stretching region which is quite similar, both in relation to the intensity and the shape of the bands, with respect to that of alumina. However, the main OH stretching band is increased a little bit in intensity and is shifted down to 3725 cm^{-1}. The high frequency components are less evident than on alumina, while more absorption is present in the region 3600–3400 cm^{-1}.

Like for alumina, the adsorption of CO on BaA produces two νCO bands (Fig. 13). The stronger band at higher coverages shifts from 2153 to ~2168 cm^{-1} upon decreasing in intensity with warming in vacuum. The weaker band shifts from ~2180 to ~2188 cm^{-1}. The analysis of the OH stretching region (Fig. 14) shows that, in this case, only part of the νCO band at

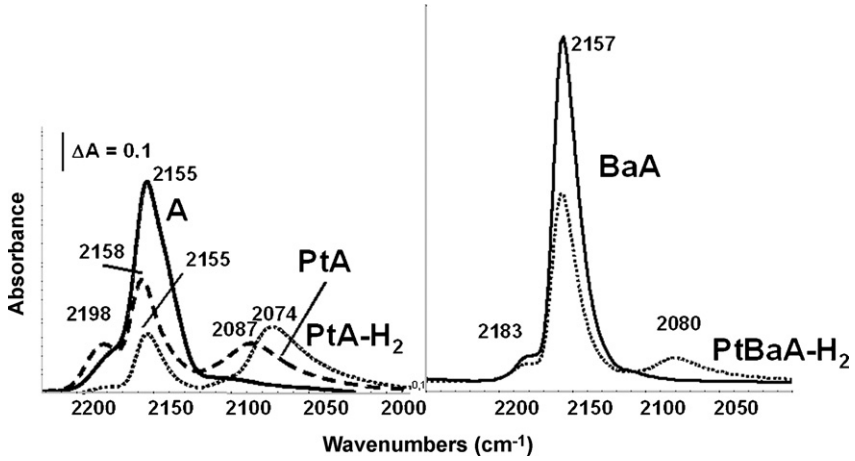

Fig. 10. Comparison of the FT-IR spectra of CO adsorbed on A, PtA unreduced and reduced (left) and BaA and PtBaA (right) after contact at 140 K and following outgassing at 150 K (left), the absorbance scale is the same for all spectra.

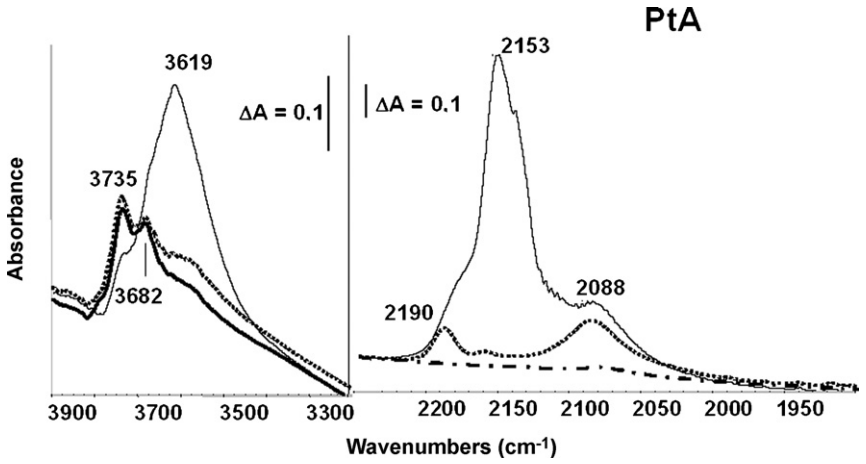

Fig. 11. FT-IR spectra of PtA (left, OH stretching region), and of CO adsorbed on PtA (right), after activation (heavy line), after short contact with CO at 140 K (light line) and after outgassing at 190 K (point line) and at 373 K (dashed line).

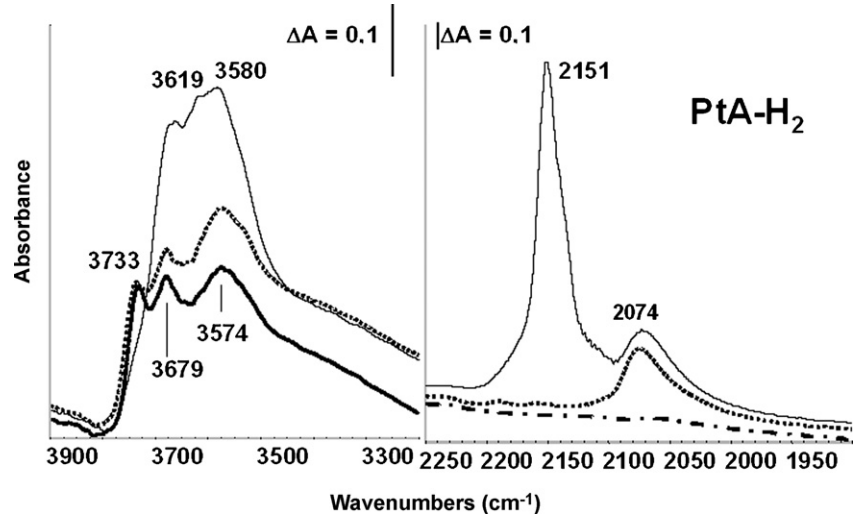

Fig. 12. FT-IR spectra of reduced PtA (left, OH stretching region), and of CO adsorbed on A (right), after activation (heavy line), after short contact with CO at 140 K (light line) and after outgassing at 190 K (point line) and at 373 K (dashed line).

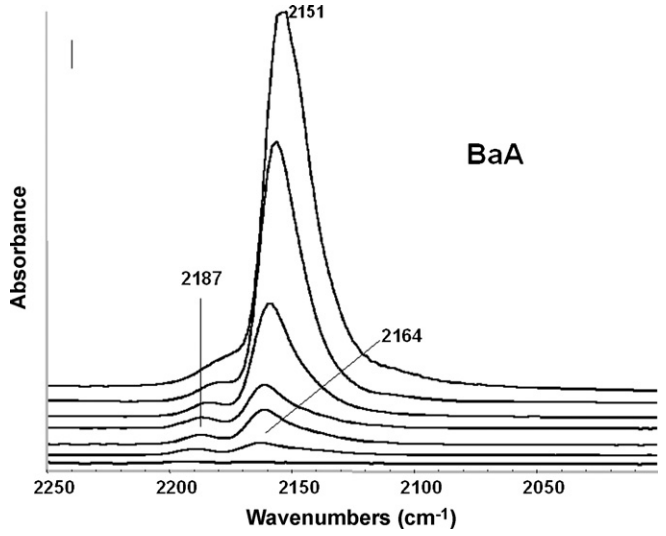

Fig. 13. FT-IR spectra of CO adsorbed on BaA at 140 K in contact with CO gas, and after outgassing at increasing temperatures from 140 to 203 K (from up to down). The spectrum of the activated catalyst has been subtracted.

2150–2170 cm^{-1} is due to CO H-bonded to OHs. In fact, the νOH band at 3725 cm^{-1} shifts to 3630 cm^{-1} at the highest CO coverages, when the maximum of the νCO band is in the region 2155–2150 cm^{-1}, still very strong (Fig. 14). This shift ($\Delta\nu OH \sim 95\ cm^{-1}$) indicates that these OH groups are definitely less acidic than those of alumina.

At lower coverages the band at 3725 cm^{-1} is fully restored but the νCO band is still evident in the range 2165–2155 cm^{-1}. The comparison of the spectra recorded on BaA and on A in the same conditions (Fig. 15) shows a definitely stronger band on BaA than on A. This strongly suggests that, in the case of BaA, a νCO band due to Ba^{2+} –CO carbonyl species may be superimposed to that of H-bonded CO. Ba carbonyl species have been reported to adsorb in this region [22] in agreement with the weak Lewis acidity of Ba ions on solid surfaces [41,43].

To have a further evidence of what happens on the surface of BaA we have also investigated and compared the spectra obtained after adsorption of a very low pressure (less than 0.5 Torr for 1 min, Fig. 16) of acetonitrile on BaA and on A.

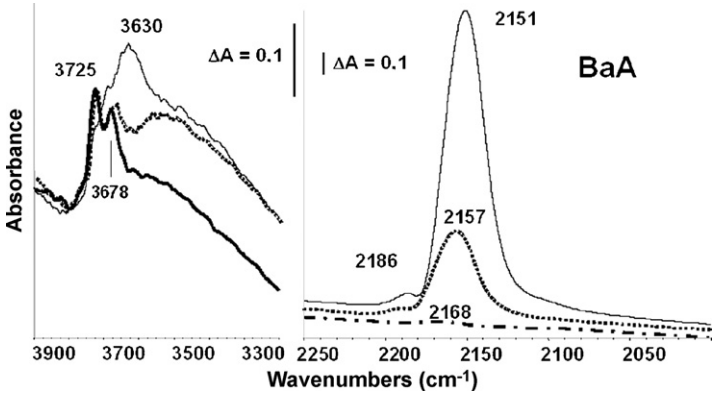

Fig. 14. FT-IR spectra of BaA (left, OH stretching region), and of CO adsorbed on BaA (right), after activation (heavy line), in contact with CO at 140 K (light line) and after outgassing at 140 K (point line) and at 200 K (dashed line).

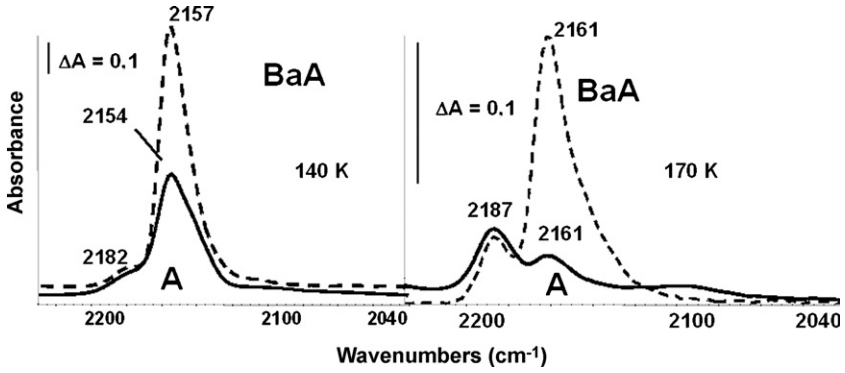

Fig. 15. Comparison of the FT-IR spectra of CO adsorbed on A and BaA after outgassing at 140 K (left) and 170 K (right).

Acetonitrile may probe both surface acidity and surface basicity [44,45]. In this region acetonitrile in CCl_4 solution shows a strong doublet at 2292, 2255 cm^{-1}, where the latter band is definitely stronger than the former. This doublet is due to the Fermi resonance between the C≡N stretching and a $\delta CH_3 + \nu C–C$ combination. The virtual position of the CN stretching fundamental shifts upwards by increasing electron withdrawal from the N lone pair upon adsorption, and this causes the experimental position of both components of the doublet to shift up. Simultaneously, however, also the relative intensities of the two components progressively inverts [46]. As a result of the presence of very strong Lewis sites, on alumina acetonitrile gives rise to a strongly shifted doublet at 2331 and 2302 cm^{-1} [47], with the former component more intense. This doublet is assigned to acetonitrile species coordinated on Al^{3+} ions. In the same conditions on BaA these absorptions are very weak and a very strong doublet is present at 2296 and 2255 cm^{-1}, i.e. very weakly shifted up. In these conditions, this doublet can be attributed to acetonitrile coordinated on Ba^{2+} ions. These ions, due to the low charge and the large size, are poorly polarizing, and give rise to very limited shifts of the vibrational modes of adsorbed bases [41,43]. On BaA a broad absorption, shifted into two components, is also formed in these conditions in the range 2050–2200 cm^{-1}. These bands are typically formed on the surface of basic materials and are attributed to CN stretching of acetonitrile enolate anions, $–CH_2–CN$. These experiments evidence that the predominant behavior of the surface of BaA is associated to highly ionic $Ba^{2+}–O^{2-}$ bonds, which display weak Lewis acidity and strong basicity, as typical of the alkali-earth oxides [44–46].

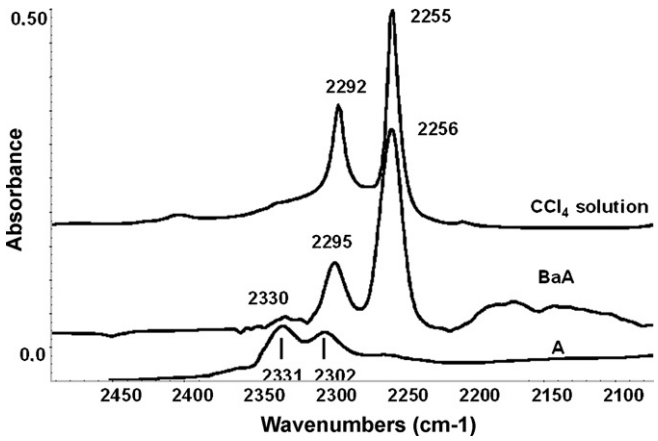

Fig. 16. Comparison of the FT-IR spectra of acetonitrile adsorbed on A and BaA at very low coverages. The spectra of the activated catalysts have been subtracted.

3.9. Surface hydroxy groups and CO adsorption on Pt–Ba–γ-Al_2O_3, oxidized, reduced and sulphated

The spectrum of PtBaA in the OH stretching region, before and after reduction (Fig. 17) is similar to that of BaA. However,

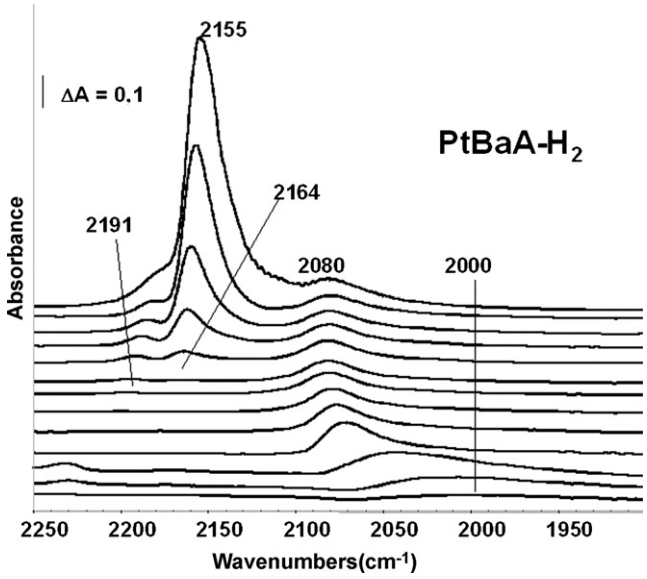

Fig. 17. FT-IR spectra of CO adsorbed on PtBaA, reduced, at 140 K in contact with CO gas, and after outgassing at increasing temperatures from 140 to 273 K (from up to down). The spectrum of the activated catalyst has been subtracted.

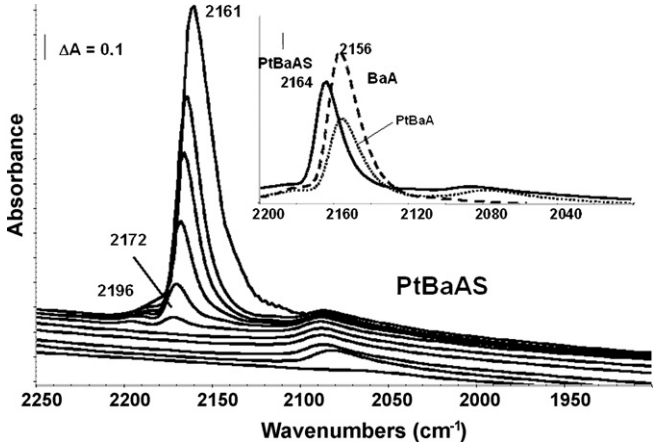

Fig. 18. FT-IR spectra of CO adsorbed on PtBaAS, reduced, at 140 K in contact with CO gas, and after outgassing at increasing temperatures from 140 to 273 K (from up to down). The spectrum of the activated catalyst has been subtracted. In the insert: comparison of the spectra of CO adsorbed on PtBaAS, PtBaA and BaA after outgassing at 160 K.

again reduction in hydrogen seems to cause the more complete disappearance of the high frequency νOH components (3790 and 3770 cm^{-1}). The adsorption of CO on the reduced sample (Fig. 16) shows the formation of the bands due to Al^{3+}–CO (2192–2185 cm^{-1}), superimposed Ba^{2+}–CO and OH$\cdots$ CO species (2170–2150 cm^{-1}) and Pt^0–CO carbonyls (2090–2000 cm^{-1}). The band of Ba carbonyls and H-bonded species is definitely lower in intensity than that detected on BaA, confirming that the presence of Pt results in a decrease of the amount of dispersed Ba, pushing Ba to segregate. The band of Pt carbonyls is observed at higher frequency than on reduced PtA, suggesting that Pt is less dispersed in the presence of Ba. In fact Ba tends to limit the ability of the support to disperse Pt, just because Pt and Ba compete in the interaction on the active sites of alumina.

In Fig. 5 the spectrum of PtBaAS sample is shown. After treatment in the presence of SO_2 the bands of carbonate species are totally disappeared, while a strong complex band with components at 1190, 1123 and 1086 cm^{-1} is formed. This spectrum is similar to that of bulk $BaSO_4$ [48,49]. However, the broadness of the features and the presence of additional components (like a shoulder near 1245 cm^{-1}) suggest that surface Ba sulphates are also very likely present, in agreement with the results reported recently by Abdulhamid et al. [50]. The spectrum in the OH stretching region (Fig. 6) does not seem to be strongly influenced by sulphation.

In Fig. 18 the spectra of CO adsorbed on the sulphated catalyst PtBaAS are reported. It is similar to that of PtBaA, but with the more intense band markedly shifted upwards, now shifting from 2161 to 2172 cm^{-1} upon outgassing. This shows that sulphation perturbs significantly the state of dispersed Ba^{2+} ions, significantly enhancing their Lewis acidity, what results in a stronger shift up of νCO of adsorbed carbon monoxide. On the contrary, sulphation does not affect significantly the carbonyls on Pt.

4. Discussion

4.1. γ-Alumina

The results concerning the surface hydroxy groups and the adsorption of CO on our γ-Al_2O_3 sample substantially agree with those reported in the previous literature, as reviewed recently [16,22,45,51]. The spectrum in the OH stretching region presents four resolved features, as typical for γ-Al_2O_3 samples, at 3790, 3770, 3730 and 3675 cm^{-1}. Previous [52,53] and more recent [54] data obtained in one of our laboratories were based on the comparison of the OHs spectra of transitional alumina as with those of other spinel type sesquioxides (as γ-Fe_2O_3 and β-Ga_2O_3) and of stoichiometric and non-stoichiometric spinels (like Mg- and Zn-aluminates and ferrites, and Ni aluminates) with those of the corundum-type sesquioxides (α-Al_2O_3, α-Fe_2O_3 and α-Ga_2O_3). These studies suggested that the higher frequency doublet is due to terminal hydroxy groups bonded to Al ions in a tetrahedral-like environment, the splitting being associated to vacancies with respect to the spinel-type composition. The band at 3730 cm^{-1}, instead, is present also at the surface of α-Al_2O_3 and of stoichiometric spinels, and is consequently likely due to terminal OHs on Al ions in octahedral-like environment.

Our data show that carbon monoxide adsorbed at low temperature causes the full but fully reversible disappearance of the high frequency components at 3790 and 3770 cm^{-1}, and the only partial, but fully reversible, perturbation of the band at 3730 cm^{-1}. On the contrary, the band at 3675 cm^{-1} appears fully unperturbed by CO. These data confirm that the two highest frequency OH stretching bands on alumina are due to hydroxy- groups which are well exposed and available to interaction with weak bases, while the lower frequency ones seem to be fully inactive. The band centered at 3730 cm^{-1} could in fact be due to the superimposition of two bands due to two different species only one of which is available to interact with CO. Additional experiments performed with stronger

bases like acetonitrile and pyridine [55] indicate that actually the band at 3730 cm^{-1} may be fully perturbed by bases while confirm that the band at 3675 cm^{-1} is fully inactive in the adsorption. This picture is quite in contrast with that reported by other authors [56].

4.2. Pt–γ-Al_2O_3

The data concerning CO adsorption over Pt–γ-Al_2O_3 are in good agreement with those reported in the literature for similar samples characterized by low Pt loading. The unreduced sample shows evident the feature of CO terminal carbonyls over highly dispersed Pt particles but also features likely due to carbonyls of Pt ions in high oxidation state. In agreement, also XPS data show both oxidized and reduced Pt. The reduction in hydrogen causes the formation or even more dispersed Pt particles, characterized by the formation of terminal carbonyls with a lower CO stretching frequency. The nature of these species being due to particles more than isolated atoms or clusters is confirmed by the shift down of the band of terminal carbonyls at low coverages, associated to the disappearance of dipole–dipole coupling. However, the coupled interpretation of IR and TEM data suggest that relatively large particles (∼10 nm size) are present together smaller ones, whose size is very few nanometers.

The analysis of the OH stretching region shows that the presence of Pt in the unreduced catalyst corresponds to the partial disappearance of the higher frequency OH stretching bands, which, according to the above description, are associated to Al ions in tetrahedral environment. It seems likely that these OHs are disappeared due to cation exchange, i.e. the protons should be replaced by Pt ions. The reduction causes the full disappearance of these OHs but some hydrogen-bonded groups are formed. On the contrary, the OH stretching band at 3730 cm^{-1} is apparently not decreased in intensity but shifted a little bit up, to 3735 cm^{-1}. This band is also apparently weakened in its basicity, being shifted of $\Delta\nu \sim 115$ cm^{-1} upon H–bonding with CO instead of $\Delta\nu \sim 135$ cm^{-1} for the same band in γ-Al_2O_3.

These data suggest that the location of Pt species, probably the smallest particles, on the alumina surface is ‘‘selective’’, substituting or exchanging the OH sites located on tetrahedral Al species, while they only perturb the OHs located over octahedral Al species.

4.3. Ba–γ-Al_2O_3

The CO and acetonitrile adsorption data show that the surface of BaA is largely covered by Ba^{2+} ions. These ions have a weak Lewis acid behavior, thus resulting in small shifts up of the CO stretching band of adsorbed carbon monoxide (2150–2168 cm^{-1}) and of acetonitrile. XPS and IR data indicate that these species are likely predominantly associated to surface carbonate species. The IR spectra show that the features due to surface exposed Al ions (Lewis sites detected by CO and by acetonitrile), present in the spectra of A, do not disappear in those of BaA. However, the high frequency OH stretching bands of alumina, found weak at 3790 and 3770 cm^{-1} in the spectra of A, disappear in the spectra of BaA. The OH stretching band observed at 3730 cm^{-1} in the spectra of A is slightly shifted, to 3725 cm^{-1}, on BaA: however, the acidity of these OHs is definitely reduced. These data show that in the case of BaA, besides the presence of small particles of bulk $BaCO_3$, evident in the XRD, the dominant surface species is constituted, in our conditions, by a Ba oxide/carbonate phase dispersed selectively in some surface site of alumina, mostly substituting or perturbing the OHs bonded to tetrahedral Al cations. This species is strongly basic and presents also weak Lewis acidity, as typical of strongly ionic, low charge and large size metal cation oxides [45,46]. The essential perturbation of the surface features of alumina by Ba species are similar to those are also produced by Pt species. This suggests that the two metal species interact competitively with the surface sites of alumina.

4.4. Pt–Ba–γ-Al_2O_3

The co-deposition of Pt and Ba on alumina produces materials whose properties are quite the sum of those of Pt-alumina and of Ba-alumina. The position of the band of carbon monoxide adsorbed on Pt, as well as the size of the particles observed by TEM, does not change very much with the copresence of barium. The Pt XPS spectra also show a weak effect due to the copresence of Ba ions. This effect is possibly electronic, as shown in other cases [31,38], although its association to moderate changes in the average particle size is not excluded. What is certainly relevant, however, is the close proximity, on the catalyst surface, of Pt and Ba species, that allows Pt to catalyze the reduction of NxOy species adsorbed over Ba-containing surface, which is one of the key mechanistic features of the NSR process [57].

The contact of the catalyst with small SO_2 pressure results in the full disappearance of the features of the carbonate species and in the appearance of sulphate species. IR study of adsorbed CO provides evidence of the predominance of dispersed Ba species also in the case of the sulphated sample. The Lewis acidity of Ba^{2+} ions is however definitely increased by sulphation (the band of adsorbed CO shifts up of near 10 cm^{-1}). This suggests that the predominant surface species in the sulphated sample is dispersed Ba sulphate, whose cations are more acidic than those of the corresponding surface oxide/carbonate phase.

5. Conclusions

The data reported here provide evidence for the predominance of the dispersed Ba phases (oxide/carbonate in dry SO_x-free and NO_x-free conditions, sulphate after contact during activation with SO_2) in our Pt–Ba–γ-Al_2O_3 that shows good activity and selectivity in NO_x storage and reduction. A Ba oxide/carbonate phase dispersed selectively in some surface site of alumina, mostly substituting or perturbing the OHs bonded to tetrahedral Al cations, is formed. This species, that involves ∼95% of the Ba ions in our catalyst preparation, is

strongly basic and presents also weak Lewis acidity, as typical of strongly ionic, low charge and large size metal cation oxides. Only a small fraction of this ''surface monolayer'' phase, ~20% is actually active in NO_x adsorption. The presence of Ba species does not change very much the characteristics of surface Pt species, although in some ways the two metal species likely ''compete'' for interaction on the same sites of the alumina support. As a result, Pt and Ba species are in close proximity on the catalyst surface, and this allows Pt to catalyze the reduction of NxOy species adsorbed over Ba-containing surface sites, which is one of the key mechanistic features of the NSR process.

Acknowledgement

Prof. L. Lietti, Politecnico di Milano, is gratefully acknowledged for helpful suggestions and for the utilization of the transient catalytic conversion plant.

References

[1] K. Kato, H. Nohira, K. Nakanishi, S. Iguchi, T. Kihara, H. Muraki, Eur. Patent application 0573672 A1 (1993) to Toyota.
[2] N. Takahashi, H. Shinjoh, T. IIjima, T. Suzuki, K. Yamazaki, K. Yokota, H. Suzuki, N. Miyoshi, S. Matsumoto, T. Tanizawa, T. Tanaka, S. Tateishi, K. Kasahara, Catal. Today 27 (1996) 63.
[3] European Patent Application No. 01107629.6 (2001) Toyota.
[4] K. Nakatani, S. Hirota, S. Takeshima, K. Itoh, T. Tanaka, SAE Paper SP-1674 (2002) 2002-01-0957.
[5] W.S. Epling, L.E. Campbell, A. Yezerets, N.W. Currier, J.E. Parks II, Catal. Rev. 46 (2004) 163–245.
[6] F. Prinetto, G. Ghiotti, I. Nova, L. Lietti, E. Tronconi, P. Forzatti, J. Phys. Chem. B 105 (2001) 12732.
[7] T. Lesage, C. Verrier, P. Bazin, J. Saussey, M. Daturi, Phys. Chem. Chem. Phys. 5 (2003) 4435.
[8] P.T. Fanson, M.R. Horton, W.N. Delgass, J. Lauterbach, Appl. Catal. B: Environ. 46 (2003) 393.
[9] T. Lesage, C. Verrier, P. Bazin, J. Saussey, S. Malo, C. Hedouin, G. Blanchard, M. Daturi, Topics Catal. 30/31 (2004) 31.
[10] J.A. Anderson, Z. Liu, M. Fernandez Garcıa, Catal. Today 113 (2006) 25–33.
[11] T. Szailer, Ja H. Kwak, Do H. Kim, J.C. Hanson, C.H.F. Peden, J. Szanyi, J. Catal. 239 (2006) 51–64.
[12] H. Abdulhamid, J. Dawody, E. Fridell, M. Skoglundh, J. Catal. 244 (2006) 169–182.
[13] B.C. Lippens, J.H. deBoer, Acta Crystallogr. 17 (1964) 1312.
[14] K. Sohlberg, T.S. Pantelides, S.J. Pennycook, J. Am. Chem. Soc. 123 (2001) 26.
[15] X. Krokidis, P. Raybaud, A.-E. Gobichon, B. Rebours, P. Euzen, H.J. Toulhoat, Phys. Chem. B 105 (2001) 5121.
[16] J.F. Lambert, M. Che, J. Mol. Catal. A: Chem. 162 (2000) 5.
[17] X. Liu, R.E. Truitt, J. Am. Chem. Soc. 119 (1997) 9856.
[18] J. Fripiat, L. Alvarez, S. Sanchez Sanchez, E. Martinez Morades, J. Saniger, N. Sanchez, Appl. Catal. A: Gen. 215 (2001) 91.
[19] M. Digne, P. Sautet, P. Raybaud, P. Euzen, H. Toulhoat, J. Catal. 211 (2002) 1.
[20] D.T. Lundie, A.R. McInroy, R. Marshall, J.M. Winfield, P. Jones, C.C. Dudman, S.F. Parker, C. Mitchell, D. Lennon, J. Phys. Chem. B 109 (2005) 11592.
[21] H. Knözinger, S. Huber, J. Chem. Soc., Faraday Trans. 94 (1998) 2047.
[22] K.I. Hadjiivanov, G.N. Vayssilov, Adv. Catal. 47 (2002) 307.
[23] C.D. Wagner, NIST X-ray Photoelectron Spectroscopy Database, Gathersburg, 1986.;
C.D. Wagner, A.V. Naumkin, A. Kraut-Vass, J.W. Allison, C.J. Powell, J.R. Rumble Jr., NIST Standard Reference Database 20, Version 3.4 (Web Version), http://srdata.nist.gov/xps/.
[24] L. Lietti, P. Forzatti, I. Nova, E. Tronconi, J. Catal. 204 (2001) 175–191.
[25] R.D. Shannon, C.T. Prewitt, Acta Crystallogr. B 25 (1969) 925.
[26] M. Piacentini, M. Maciejewski, A. Baiker, Appl. Catal. B: Environ. 60 (2005) 265–275.
[27] C.M.L. Scholz, V.R. Gangwal, M.H.J.M. de Croon, J.C. Schouten, J. Catal. 245 (2007) 215–227.
[28] J.F. Moulder, W.F. Stickle, P.E. Sobol, K.D. Bomben, Handbook of X-ray Photoelectron Spectroscopy, PerkinElmer Corporation, 1992.
[29] G. Corro, J.L.G. Fierro, R. Montiel, F. Bañuelos, J. Mol. Catal. A: Chem. 228 (2005) 275.
[30] S. Damyanova, J.M.C. Bueno, Appl. Catal. A: Gen. 245 (2003) 135.
[31] K. Persson, A. Ersson, K. Jansson, J.L.G. Fierro, S.G. Järås, J. Catal. 243 (2006) 14.
[32] G.J. Siria, J.M. Ramallo-López, M.L. Casella, J.L.G. Fierro, F.G. Requejo, O.A. Ferretti, Appl. Catal. A: Gen. 278 (2005) 239.
[33] M. Casapu, J.-D. Grunwaldt, M. Maciejewski, A. Baiker, S. Eckhoff, U. Göbel, M. Wittrock, J. Catal. 251 (2007) 28–38.
[34] J.H. Park, M.K. Lee, C.K. Rhee, W.W. Kim, Mater. Sci. Eng. A 375–377 (2004) 1263.
[35] H.Y. Zhu, J.D. Riches, J.C. Barry, Chem. Mater. 14 (2002) 2086–2093.
[36] L. Castoldi, I. Nova, L. Lietti, P. Forzatti, Catal. Today 96 (2004) 43–52.
[37] J.M. Alía, Y. Díaz de Mera, H.G.M. Edwards, P. González Martín, S. López Andrei, Spectrochim. Acta A: Mol. Biomol. Spectrosc. 53 (1997) 2347.
[38] E.A. Schauble, P. Ghosh, J.M. Eiler, Geochim. Cosmochim. Acta 70 (2006) 2510.
[39] W.P. Griffith, J. Chem. Soc. A (1970) 286.
[40] P. Pasierb, S. Komornicki, M. Rokita, M. Rękas, J. Mol. Struct. 596 (2001) 151.
[41] G. Busca, V. Buscaglia, M.P. Leoni, P. Nanni, Chem. Mater. 6 (1994) 955.
[42] L.-C. De Ménorval, A. Chaqroune, B. Coq, F. Figueras, J. Chem. Soc., Faraday Trans. 93 (1997) 3715.
[43] G. Busca, C. Cristiani, P. Forzatti, G. Groppi, Catal. Lett. 31 (1995) 65.
[44] J.C. Lavalley, Catal. Today 27 (1996) 377.
[45] G. Busca, in: J.L.G. Fierro (Ed.), Metal Oxides: Chemistry and Applications, CRC Press, Boca Raton, FL, USA, 2005, p. 247.
[46] G. Busca, Phys. Chem. Chem. Phys. 1 (1999) 723.
[47] H. Knözinger, H. Krietenbrink, J. Chem. Soc., Faraday Trans. I 71 (1975) 2421.
[48] P. Dawson, M.M. Hargreave, G.R. Wilkinson, Spectrochim. Acta 33A (1977) 83.
[49] H. Bala, W. Fu, Y. Guo, J. Zhao, Y. Jiang, X. Ding, K. Yu, M. Li, Z. Wang, Colloids Surf. A: Physicochem. Eng. Aspects 274 (2006) 71.
[50] H. Abdulhamid, E. Fridell, J. Dawody, M. Skoglundh, J. Catal. 241 (2006) 200.
[51] G. Busca, Chem. Rev. 107 (2007) 5366.
[52] G. Busca, V. Lorenzelli, V. Sanchez Escribano, R. Guidetti, J. Catal. 131 (1991) 167.
[53] G. Busca, V. Lorenzelli, G. Ramis, R. Willey, Langmuir 9 (1993) 1492.
[54] G. Busca, in: S.D. Jackson, J.S.J. Hargreaves (Eds.), Oxides and Oxidation Catalysis, Wiley (2008), in press.
[55] Unpublished results.
[56] H. Knözinger, in: G. Ertl, H. Knözinger, J. Weitkamp (Eds.), Handbook of Heterogeneous Catalysis, 2, Wiley–VCH, Weinheim, 1997, pp. 707–732.
[57] I. Nova, L. Lietti, L. Castoldi, E. Tronconi, P. Forzatti, J. Catal. 239 (2006) 244–254.